HAL open science

A Microrobotic Approach for the Intuitive Assembly of Industrial Electrooptical Sensors Based on Closed-Loop Light Feeling

Ahmad Awde, Mokrane Boudaoud, Mélanie Macioce, Stéphane Regnier, Cédric Clevy

To cite this version:

Ahmad Awde, Mokrane Boudaoud, Mélanie Macioce, Stéphane Regnier, Cédric Clevy. A Microrobotic Approach for the Intuitive Assembly of Industrial Electrooptical Sensors Based on Closed-Loop Light Feeling. IEEE/ASME Transactions on Mechatronics, 2022, pp.1 - 10. hal-03812983v2

HAL Id: hal-03812983

https://hal.science/hal-03812983v2

Submitted on 18 Oct 2023

HAL is a multi-disciplinary open access archive for the deposit and dissemination of scientific research documents, whether they are published or not. The documents may come from teaching and research institutions in France or abroad, or from public or private research centers.

L'archive ouverte pluridisciplinaire **HAL**, est destinée au dépôt et à la diffusion de documents scientifiques de niveau recherche, publiés ou non, émanant des établissements d'enseignement et de recherche français ou étrangers, des laboratoires publics ou privés.

A Micro-Robotic Approach For the Intuitive Assembly of Industrial Electro-Optical Sensors Based on Closed-Loop Light Feeling

Ahmad Awde, Mokrane Boudaoud, Mélanie Macioce, Stéphane Régnier, and Cédric Clévy

***Abstract*—This article deals with an original haptic teleoperation and human-robot interaction (HRI) for microrobotic tasks involving optics and more generally light information. It aims to demonstrate the proof of concept of using light information in haptic teleoperation for component alignment with submicrometer accuracy. The case study focuses on the alignment of a laser optical fiber on the active surface of a photodiode using a microrobotic system and a pantograph. Since an alignment error of $1\ \mu m$ leads to a loss of more than $35\ \%$ in signal transmission, it is shown that the transparency of the pantograph is a key element for the success of the operation. A user evaluation is performed to quantify the interest and acceptability of the different HRI scenarios proposed in this work. The result shows the effectiveness of the methods when the interface transparency is managed with a disturbance observer. The HRI allows the human to experience small variations of light, typically a few μW, over a large range, typically several hundred μW. This capability enables the participant to intuitively align the optical fiber in the region of interest with a sub-μm accuracy and a success rate of about 94.7%.**

***Index Terms*—Micro-assembly, automation, collaborative work, micro-robotics, opto-electronics devices.**

I. Introduction

HIGH-precision robotic positioning and assembly of small-scale components whose size typically ranges between the millimeter and the micrometer scale are highly demanded tasks because they open the door to many innovative product architectures [1]–[4]. On the one hand, productive machines, such as flip-chip ones, have been optimized to achieve dedicated tasks to the manufacturing of mass-produced, high-cost products, typically microelectronics and biomedical devices [5]. On the other hand, manual assembly is also widespread because it takes advantage of the user's expertise and capacity to adapt the manipulation protocol to environmental disturbances and the peculiarities of the task. This approach is especially applied to small series of products where adaptation to product complexity and personalizing is of importance to ensure the success of the assembly [6]–[8].

Many complex, high added value products have been introduced to the market, such as for instrumentation purposes (e.g., near-field probing and measurement through light), minimally invasive surgery, and inspection of small scale cavities. The key limitation lies in the scaling up of their production, notably because they require a succession of many challenging assembly tasks that must be ensured with dexterity and sub-micrometer accuracy. Current practices mainly consist in trial-and-error and dedicated procedures requiring a long and tedious training of the operators so that they can reach enough skills in a specific context of production. Microrobotic systems offer the possibility to perform precise positioning with sub-micrometer accuracy of robotic axes [9] [10] and manipulation tools [11] [12]. Human-robot interaction (HRI) using micro-positioning robots brings the human expertise in the control loop while taking advantage of the precision and the repeatability of micro-positioning robots. HRI also brings relevant and efficient solutions to deal with complex environments tasks [13] and for unforeseen situations [14] which is the typical case among microrobotic applications [15]. This requires the use of bilateral haptic devices able to provide a high fidelity interactions via force feedback [16]. In this scope, what physical sensory feedback to be used, how to use it to take advantage of human sensorimotor capabilities, and the acceptability of the operator to the physical sensory feedback appear as a key paradigm.

This article investigates an original HRI approach for the intuitive micro-assembly of electro optical components where the light intensity, measured by a photodiode, is used as haptic feedback. Indeed, many startup companies involved in deep electronics technologies use electro optical components. These components, which transform light or a change in light into an electronic signal, are core elements of modern instrumentation technologies [17] and directly face the scale-up of their production previously mentioned. To successfully achieve the assembly of such components, the active alignment is a standard method. It consists in making the electro optical sensor working during its assembly and to use its output, generally a light intensity, as feedback to the robotic system and/or the user. Bettahar et *al*. [18] proposed an automated robotic approach for optical alignment. The full automation is, however, not the main standard of startup companies. For small series production with a constant high-quality requirement of the final products, some key assembly steps are usually

Ahmad AWDE and Cédric CLEVY are with the AS2M (Department of Automatic Control and Micro-Mechatronic Systems), Institut FEMTO-ST UMR 6174, Univ. Bourgogne Franche-Comté, ENSMM, CNRS, F-25000, Besançon, France. (e-mail: ahmad.awde, cedric.clevy@femto-st.fr). Ahmad AWDE, Mokrane BOUDAOUD and Stéphane REGNIER are with Sorbonne University, Institut des Systèmes Intelligents et de Robotique, UMR 7222, ISIR, F-75005 Paris, France (e-mail: ahmad.awde, mokrane.boudaoud, stephane.regnier@isir.upmc.fr) Mélanie MACIOCE is with AUREA TECHNOLOGY Company. (e-mail: melanie.macioce@aureatechnology.fr)

done in a tele-operated mode where a human expert worker continuously achieves adaptations based on measurements and observations followed by a trial-and-improvement approach.

To the best of our knowledge, the use of light intensity as a haptic feedback for the micro-assembly and alignment of electro optical components via a HRI has not been addressed in the literature before despite the fact that many robotic tasks use light information. To achieve sub-micrometer accuracy in alignment, haptic interfaces must reflect light intensity variations as forces to the user without artifact. However, the dynamics of motion of haptic interfaces have a significant influence on the sensation of force. Therefore, the transparency of the haptic interface is a major challenge in this context. In a previous work [19], a disturbance observer (DOB) was associated with a pantograph, a parallel type of haptic interface, characterized by a large dynamic bandwidth and a low friction. The purpose of the DOB is to estimate the force that the human applies on the interface, it allows then to reject the disturbing forces that affect the transparency of the bilateral coupling.

The main contributions of this paper are as follows:

- Study of the effect of pantograph transparency on the alignment accuracy of an optical fiber with haptic light feedback.
- Proposition of HRI strategies for intuitive optical fiber alignments.
- User evaluation.

The rest of this article is organized as follows. Section II summarizes a previous work related to the pantograph modeling and DOB design. The problem formulation for the electro optical devices' alignment is described in Section III. Section IV deals with the strategy for the intuitive alignment by means of HRI relying solely on light variation feeling. Section V presents the user evaluation test to study the effectiveness of the proposed approach in terms of acceptability of the technology and performance of the tasks. Finally, Section VI concludes this article.

II. Pantograph haptic interface and disturbance observer design

The proposed HRI approach is based on the bilateral coupling between a pantograph haptic interface and a microrobotic system to sense light intensity variations as forces. This approach requires that the human operator can distinguish fine variations in light intensity through the haptic interface. In this section, the haptic interface used for bilateral coupling, the transparency issue, and the design of the DOB are presented.

A. Bilateral haptic interface and transparency issue

In [19], the modeling of a pantograph and the design of a DOB have been introduced. The pantograph (see Fig. 1 (a)) is a planar bilateral haptic interface. It has a quasi-flat frequency bandwidth in the range DC to 400 Hz, allowing the transmission of a force information in a large human kinesthetic sensing bandwidth [20]. At the contact point E, (see Fig. 1 (b)), the human operator can apply a force $F_h = \begin{bmatrix} F_{hx} & F_{hy} \end{bmatrix}$ and feels a force $F_m = \begin{bmatrix} F_{mx} & F_{my} \end{bmatrix}$ generated by the torques τ_1 and τ_4 of the two DC motors.

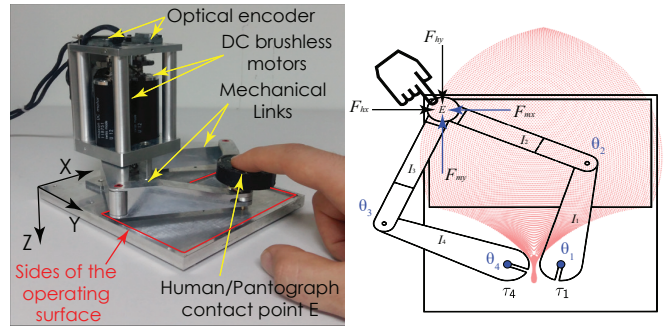

(a) (b)

Fig. 1. (a) Pantograph: a bilateral haptic interface. (b) Schematic representation of the pantograph.

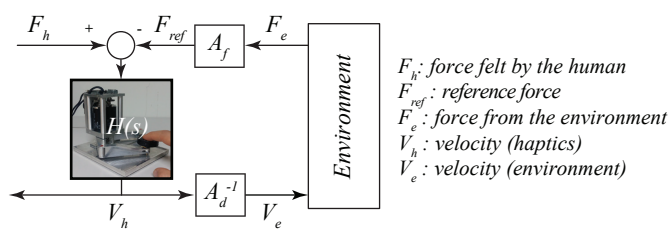

Fig. 2. Force feedback with a bilateral coupling.

The transparency of a haptic coupling refers to its ability to faithfully transmit to the operator a physical quantity (e.g., force) from the environment [21]. This property is defined as a comparison between the impedance felt by the human $Z_h = \frac{F_h}{V_h}$ and that of the environment $Z_e = \frac{F_e}{V_e}$ (see Fig. 2). The "ideal" transparency is achieved when:

$$Z_h(s) = \frac{A_f}{A_d} Z_e(s) \tag{1}$$

where s is the Laplace variable, and A_f and A_d are the force and distance amplification factors respectively. Using the scheme of Fig. 2, the impedance felt by the operator is

$$Z_h(s) = \frac{A_f}{A_d} Z_e(s) + \frac{1}{H(s)} = \frac{A_f}{A_d} Z_e(s) + M_h s + C_h \tag{2}$$

where M_h and C_h are, respectively, the mass and the viscosity factor of the haptic interface. To obtain "the ideal" transparency, the dynamic of the interface should be compensated so that M_h and C_h will no longer affect $Z_h(s)$. Therefore, (2) will be equal to (1).

B. Perturbation rejection

To design the DOB, a dynamic model of the pantograph is used (a detailed presentation of the model is given in [19])

$$M_h(q)\ddot{X} + C_h(q, \dot{q})\dot{X} = F_m - F_h, \tag{3}$$

where $M_h(q)$ and $C_h(q, \dot{q})$ are the inertia and Coriolis damping matrices of the system expressed in the task-space, F_m is the control force input, $V = \begin{bmatrix} X_E & Y_E \end{bmatrix}$ is the coordinate vector of the point E, and q is the state vector $q = [\theta_1 \ \theta_2 \ \theta_3 \ \theta_4]^T$ in the joint space (Fig. 1 (b)). The force $C_h(q, \dot{q})\dot{X}$ is negligible compared to $M_n(q)\ddot{X}$. Therefore, (3) becomes $M_h(q)\ddot{X} = F_m - F_h$.

Based on this model, a DOB is developed in [19] to estimate the force $\hat{F}_h$ that the human applies on the interface:

$$\hat{F}_h = (Q(s)(F_m + g \times M_h(q)\dot{X})) - g \times M_h(q)\dot{X} \quad (4)$$

where $Q(s) = \frac{g}{s+g}$ is a low pass filer with a cut of frequency $\omega_c = g = 540$ rad/s. It is large enough to cover the dynamic frequency range of the pantograph.

To ensure that the human operator feels the reference force F_{ref}, the block diagram of Fig. 3 is implemented. By applying the control input force $F_m = F_{ref} + \hat{F}_{inertia}$, the human operator feels the reference force $F_h = F_{ref}$.

III. Electro-optical devices' alignment: Problem formulation

A. Experimental setup

The experimental setup is shown in Fig. 4. The laser source provides a light with a wavelength $\lambda_{light} = 1550\ nm$ and an equivalent intensity $I_{light} = 850\ \mu W$. It is connected to an optical focusing system through an optical fiber. The diameter of the light beam emitted by the focusing system is $9\ \mu m$. The photodiode has an active surface of $25\ \mu m \times 25\ \mu m$. The focusing system is mounted on a XYZ nano-positioning robot (P-616-3C) with a $100\ \mu m/axis$ travel range and a resolution of $0.4\ nm$. The coarse pre-positioning is made by XYZ manual micro-positioning stages. An electronic circuit is used to process the light signal detected at the active surface of the photodiode into a voltage signal. An oscilloscope is used to visualize the output voltage of the electronic system. The laser source, the focusing system and the photodiode are parts of a photon counter made by the AUREA Technology Company in Besançon, France.

B. Light intensity map characterization

The intensity of the light captured by the photodiode depends on the position of the focusing system with respect to (w.r.t) the photodiode in X, Y and Z directions. The optical axis is in the Z direction. Fig. 5 shows experimental data highlighting the effect of the position z_p (Fig. 4 (b)) of the focusing system along the Z axis. For each fixed z_p, the light intensity is measured while moving the focusing system along Y axis and passing through the center of the active surface of the photodiode. The initial position $z_p = 0$ is selected so that the light received by the photodiode has the largest spot size, i.e. the largest region where the light intensity I_{light} is higher than 95 % of the laser source intensity. In the following, the focusing system is positioned so that $z_p = 0$. The light intensity map in the XY plane shown in Fig. 6 is experimentally obtained by a scanning process (Fig. 4 (b)). The XYZ micropositioning robot is used for a fine scanning of an area of $65 \times 65\ \mu m$. The light intensity is measured every $2\ \mu m$ displacement in X and Y directions. The measurements show that the intensity varies in the range $[0 - 900\ mV]$, where each mV corresponds to $0.94\ \mu Watt$. The maximum of the light intensity is not at the center point of the active surface of the photodiode. When getting closer to the center, the light intensity decreases to $850\ mV$.

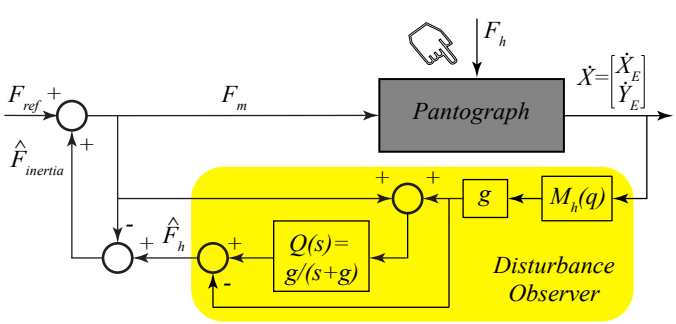

Fig. 3. Pantograph with disturbance observer (DOB).

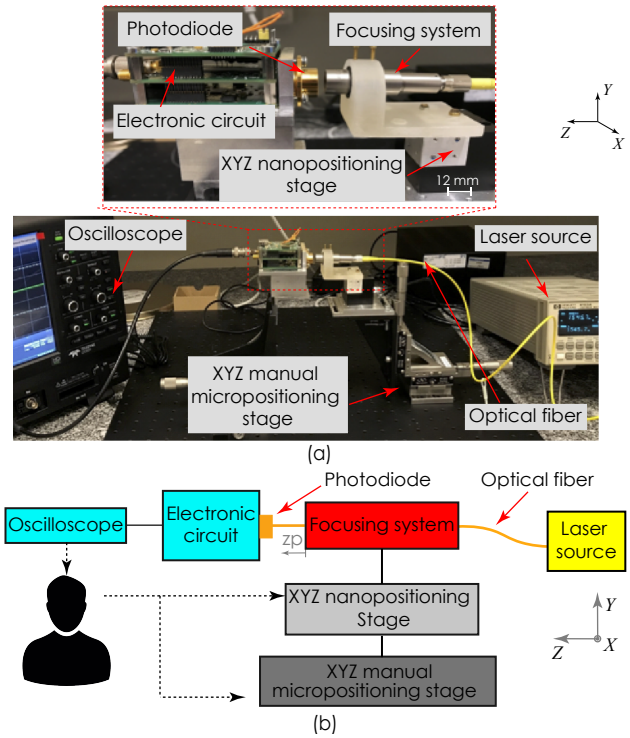

Fig. 4. Experimental setup for the optical fiber alignment w.r.t the photodiode sensor (a) and the schematic representation of the manual alignment process (b).

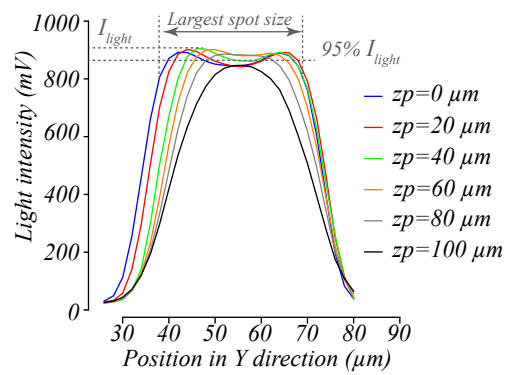

Fig. 5. Light intensity with respect to the laser beam position along Y axis for different distances Z between the optical focusing system and the photo diode active surface.

C. Optical fiber alignment and assembly issues

According to the assembly specification set up by AUREA Technology Company, the relative positioning of the focusing system w.r.t the photodiode is appropriate when the light

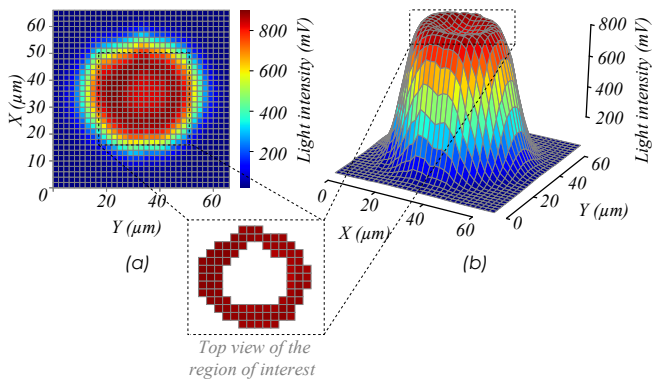

Fig. 6. Experimental light intensity map. (a) Top view and (b) 3D view.

intensity detected by the photodiode reaches at least 95 % of the laser source intensity. This region will be referred as nominal "region of interest" as shown in Fig. 6. Such an assembly induces several issues. Usually, the human operator adjusts the position of the manual positioning system based on the output signal visualized onto the oscilloscope. This is time-consuming and requires strong efforts and a high-level expertise. In addition, the shape of the light intensity map (Fig. 6) varies from a sensor to another because of the intrinsic heterogeneity resulting from the fabrication process of such devices. Finally, the relative position between the focusing system and the photodiode in the region of interest must be achieved with an accuracy at the sub μm level. The nominal region of interest, corresponds to the positions where more than 95 % of the light intensity is measured, constitutes only 7 % of the total surface of the active surface of the photodiode. However, this region doesn't exceed more than 2 % of the active surface when a high quality of the alignment is required where more than 99 % of the maximum light intensity is transmitted.

IV. Electro-Optical Devices' Alignment Based on Light Variations Feeling

This section deals with the HRI strategies based only on light variations feeling. The experimental setup and the schematic representation of the HRI are shown in Fig. 7. The focusing system is mounted on a 6 DoF serial micropositioning robot. The latter is coupled with the pantograph for motion generation along X and Y axes of the robot. The block diagram of the Fig. 3 is implemented to improve the pantograph haptic transparency.

A. Bilateral haptic coupling for optical fiber Alignment

Let's consider the block diagram of Fig. 9, where $X = [X_E \; Y_E]$ represents the coordinate vector of the contact point E and X_r the corresponding scaled position vector of the micropositioning robot. A_d represents the displacement scaling factor ($X_r = A_d^{-1}X$) and A_f the force scaling factor between F_{ref} and F_v.

The force F_v is obtained from the gradient of the light intensity $B(X_r)$ as follows:

$$F_v = \gamma \overrightarrow{grad}(B(X_r)), \tag{5}$$

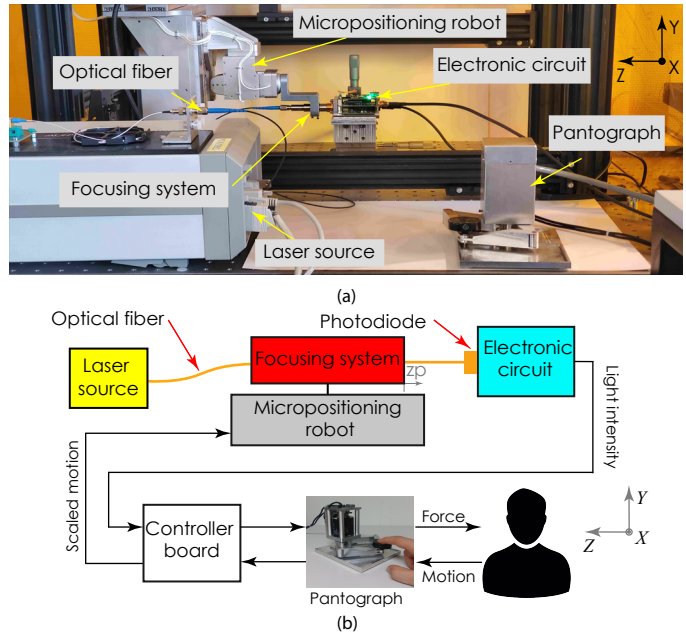

Fig. 7. (a) Experimental micro-robotic setup for the alignment of the electro-optical sensors. (b) A schematic representation of the intuitive HRI alignment proposed approach.

The scalar γ is selected so that the maximum amplitude of F_{ref} is equal to the maximum force that the pantograph can generate. Here, $\gamma = 0.002 \; N.\mu m.mV^{-1}$ so that $F_{ref} < 0.35 \; N$.

As the force F_{ref} is proportional to the gradient of the light intensity, the maximum of the light intensity is detected when $F_{ref} = 0$ as illustrated in Fig. 8 (a). The distribution of the gradient of the light intensity obtained experimentally in the XY plane of the active surface of the photodiode is shown in Fig. 8 (b).

In order to detect the region of interest for the optical fiber alignment (see section III-C), the human operator scans the laser position, at the output of the focusing system, along the active surface of the photodiode. This is done by moving the pantograph. The position of the micropositioning robot is thus adjusted by the human based solely on the force feeling. Intuitively, when the felt force is close to zero, the alignment process is completed. The key issue is the ability to feel fine variations of forces free from the effect of the pantograph's inertia.

The use of large scaling factors can affect the stability of the bilateral coupling [22]. For the stability analysis, several parameters need to be considered, namely:

- T_s: sampling time.
- A_f: force scaling factor.
- A_d: displacement scaling factor.
- M_{eq}: equivalent mass of the pantograph.

In [22], the authors studied the stability of bilateral coupled systems based on Routh-Hurwitz criterion. The contact with the environment is modeled by an equivalent stiffness K_{eq}. A necessary stability condition is derived as follows [23]:

$$\frac{A_f}{A_d} T_s^2 K_{eq} < M_{eq} \tag{6}$$

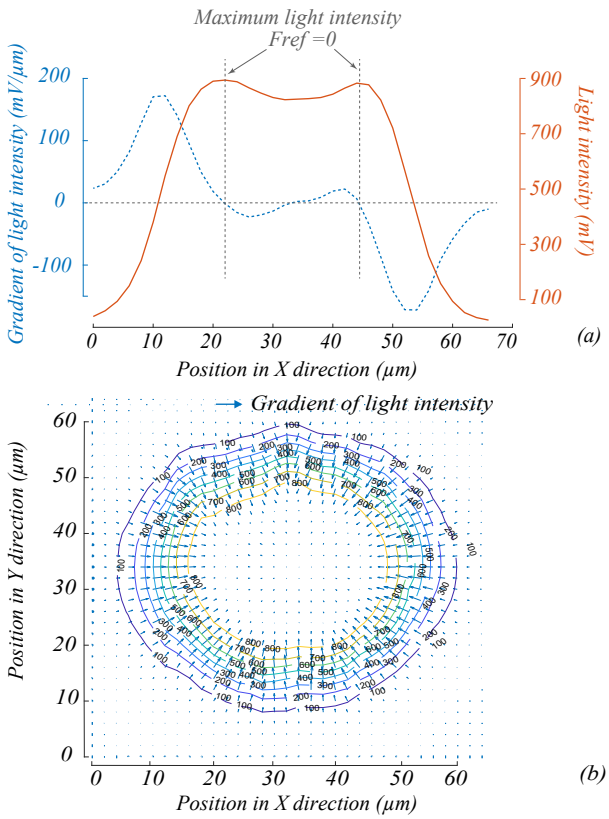

Fig. 8. (a) Light intensity with respect to the laser beam position along X axis and gradient of light intensity (at Y = 32 μm). (b) Distribution of the gradient of the light intensity in the XY plane.

In the case of the alignment of the optical fiber w.r.t the photodiode, there is no direct physical contact with the environment. Therefore, to determine the stability condition, F_v must be expressed with a linear function with respect to X_r as follows:

$$F_v = \gamma \overrightarrow{grad}(B(X_r)) < \gamma K X_r \tag{7}$$

The stability condition for the coupled system of Fig. 9 can be obtained from (6) by replacing the equivalent stiffness K_{eq} with the scalar γK, where K is a constant. The stability condition becomes:

$$\frac{A_f}{A_d} T_s^2 \gamma K < M_{eq} \tag{8}$$

The stability of the system is satisfied by choosing $K = 25\ mV.\mu m^{-2}$ which corresponds to the highest value of the derivative of $\overrightarrow{grad}(B(X_r))$ w.r.t the robot position (i.e. the

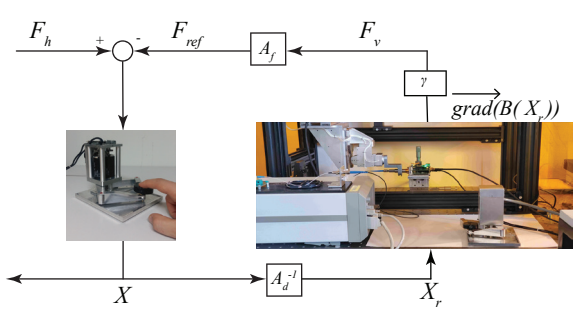

Fig. 9. Haptic coupling scheme.

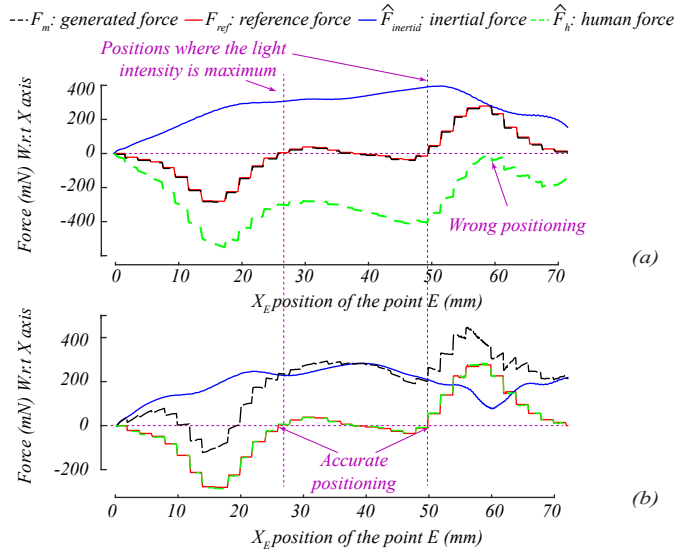

Fig. 10. Inertial force influence in fast motion scanning: comparison of the human force feeling $\hat{F}_h$ (a) without perturbation rejection ($F_m = F_{ref}$), (b) with perturbation rejection ($F_m = F_{ref} + \hat{F}_{inertia}$) (see Fig. 3).

highest slope of the dashed curve in Fig. 8 (a)) and the following parameters values $A_d = 1000$, $A_f = 1$, $T_s = 0.001\ s$, $\gamma = 0.002\ {}^{N.\mu m}/_{mV}$, $M_{eq} = 90\ g$.

B. Intuitive maximum light intensity detection

To detect the region where the light intensity is maximum, the proposed strategy is based on two steps. The first one is a coarse scanning of the laser in the XY plane made by a *fast motion* of the human fingertip. The objective is to detect roughly the region where F_{ref} is close to zero. The second step is a fine scanning around the region of interest in a *slow motion* of the human fingertip for a better alignment accuracy. In this study, the motion is considered as slow, i.e. *slow motion* designation, when the inertial force amplitude of the pantograph never exceeds $0.05\ N$. Otherwise, it is considered as *fast motion*. Whatever the type of motion, the condition $F_h = F_{ref}$ must always be satisfied for an accurate alignment.

In the sequel, the forces that are analyzed are the reference force F_{ref}, the force F_m generated at the contact point E, the haptic interface inertial force $F_{inertia}$ and the observed human force $\hat{F}_h$. To simplify the force analysis and without loss of generality, the fingertip moves the point E along the X axis only. The objective is to demonstrate the effectiveness of the observer and the perturbation rejection on the improvement of light variations feeling and consequently on the improvement of the alignment precision of the focusing system.

The data (light intensity map) provided by Aurea Technology compagny are discretized, i.e. the light intensity distribution is discrete. Thus, discrete values of the reference force appear in the graphs of Fig10 and Fig11.

1) Fast motion scanning

Without perturbation rejection, the human operator feels the force $\hat{F}_h$ that has the same shape as F_{ref}, but the influence of the inertial force $F_{inertia}$ leads to a completely wrong positioning of the laser. Indeed, in Fig. 10 (a), $\hat{F}_h = 0$ at $X_E = 59.5\ mm$. The human considers that the alignment

is correct at this position. However, the accurate alignment is at $X_E = 25.8\ mm$ or $X_E = 49.5\ mm$. For $1\ mm$ displacement of the contact point E in X or Y directions, the micropositioning robots moves by $1\ \mu m$. Therefore, the alignment error of the laser at the output of the focusing system is $10\ \mu m$. With the observer, $\hat{F}_h$ is very close to F_{ref} and the alignment accuracy is below one micrometer Fig. 10 (b).

2) Slow motion scanning

Without perturbation rejection, the effect of $F_{inertia}$ on the sensed force is less important than for fast motion scanning, but it is still present. The alignment error is equal to $0.7\ \mu m$ without the observer and perturbation rejection, while it is much smaller with the perturbation rejection.

It can be concluded that, if the operator moves the pantograph with a *slow motion*, assembly can be achieved with sub-micrometer accuracy without the need for a DOB. However, for a fast-moving scan, the DOB becomes crucial to achieve sub-micrometer accuracy during assembly. Considering that the way the haptic interface will be used differs from one human operator to another, the use of a DOB is necessary to always satisfy enough transparency for sub-micrometer assembly.

C. Navigation in the region of interest

In this experiment, the human starts from an initial position without knowing the light intensity map. The aim is to study the influence of the perturbation rejection on the positioning accuracy when the human tries to reach the maximum light intensity and navigates in the region of the interest, i.e. keeps the position of the focusing system in this region.

The results are represented in Fig. 12. The green curve represents the movement of the laser focusing system guided by the human operator. He/she only refers to the feelings of light intensity variations to make his/her decision. The results show the influence of the inertial force on the positioning of the focusing system with respect to zero force feeling. Without perturbation rejection (Fig. 12 (a)), the operator has difficulty to maintain the optical fiber in the region of interest. The navigation is improved with the perturbation rejection, as it can be seen in Fig. 12 (b).

Fig. 13 shows a box plot representation of the data collected from Fig. 12. With the perturbation rejection, the Interquartile Range (IQR) of the light intensity is $13\ mV$, the lower whisker is $850\ mV$, the minimum reached value is $812\ mV$ and the outliers are no more than $1.9\ \%$ which is fully acceptable for the alignment specifications. Whereas, without perturbation rejection, these performances are decreased: the IQR equals to $20\ mV$, the lower whisker is $830\ mV$, the minimum reached value is $651\ mV$ and there are $8\ \%$ outliers.

These results confirm the impact of the quality of the light feeling on the accuracy of the alignment process. With perturbation rejection, $97.77\ \%$ of the positions achieved reach more than $95\ \%$ of the maximum of light intensity while this value decreases to $82.1\ \%$ without perturbation rejection.

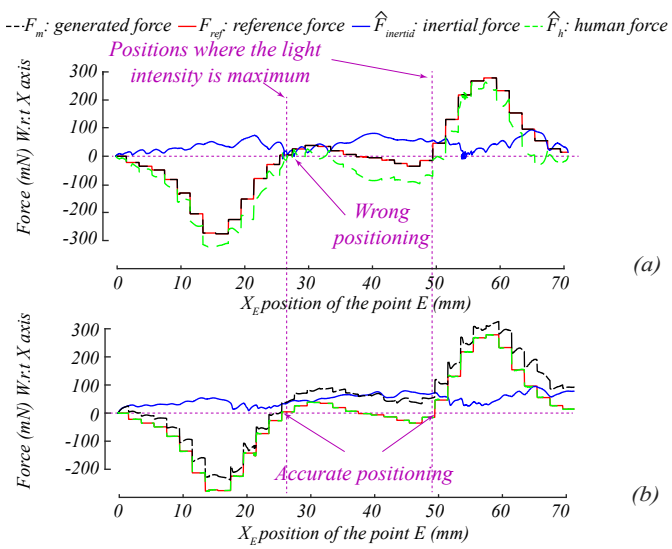

Fig. 11. Slow motion scanning: comparison of the human force feeling $\hat{F}_h$ (a) without perturbation rejection ($F_m = F_{ref}$), (b) with perturbation rejection ($F_m = F_{ref} + \hat{F}_{inertia}$) (see Fig. 3).

V. Users Evaluation

Participants are subjected to different HRI scenarios and different assembly cases represented by several typical and different light intensity distributions. The purpose of this evaluation is to compare user performance for different scenarios and to investigate user acceptability for the proposed approach.

A. Participants

The set of 14 volunteers is from FEMTO-ST institute (Besançon, France). The participants are between 23 and 55 years old. They come from different scientific backgrounds, are all right-handed and have no physical abnormalities.

B. Light intensity distributions

Photodiode sensors are the result of a non-homogeneous manufacturing process. In addition, various parameters influence the measurement of the light intensity by these sensors,

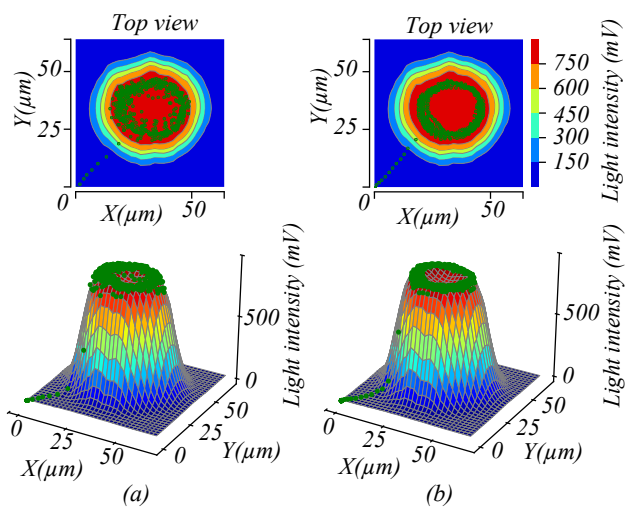

Fig. 12. Navigation without (a) and with (b) perturbation rejection. The green curve represents the movement of the laser focusing system guided by the human operator through the pantograph. The aim is to demonstrate the effect of the perturbation (inertial force) on the human decision-making for the navigation in the region of interest. When the DOB is activated, the inertial force is removed from the force felt by the human.

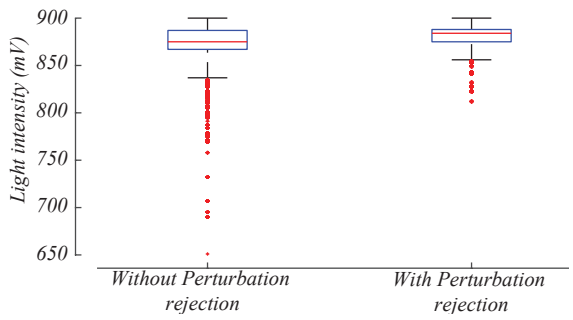

Fig. 13. Box-plot representation for the light intensity measurements.

for example the distance between the focusing system and the photodiode (Fig. 5). For these reasons, the light intensity maps are different from a sensor to another. For the user evaluation, four different types of light intensity distributions that represent typical cases resulting from different imperfections are used. They are shown in Fig. 14.

Fig. 14 (a) represents a symmetrical distribution with respect to the vertical axis passing through its center, where the global maximum value of the light intensity is located. In Fig. 14 (b), the distribution is symmetrical on the vertical axis passing through its center and the global maximum values of light intensity constitute an annular region of interest. However, in Fig. 14 (c), the local maximum light intensity values constitute a region with a global value at the edge of this region. Finally, Fig. 14 (d) represents a distribution that has three local maximum values (of which, only one is a global maximum). One of these values is in the center of the distribution while the other two are at the edge of the distribution with small variations between these two values.

C. Evaluation protocol

Experiments are conducted with one participant at a time for a total duration of approximately 60 minutes for each user. The user evaluation test is conducted in two steps:

Training step: It lasts about 10 minutes. This step aims to familiarize the participant with the haptic force feedback, which represents the variations of light intensity via the pantograph. The participant is encouraged to discern the change in light intensity corresponding to the force sensation via the haptic interface.

Identification and localization step: This step aims to identify by the user the different light intensity distributions based on the information received and to localize the position of the maximum light intensity. It consists of four different scenarios. These scenarios are distinguished according to the information received by the participant:

1) $Visual\ scenario$: It represents the industrial technique currently used as at AUREA Technologies Company. The participant only sees a slider bar, whose length corresponds to the percentage of light intensity transmission, without any insight into the global distribution of the light intensity.
2) $Haptic\ scenario$: With the pantograph, the participant experiences only light intensity changes as a force feeling without considering the disturbance forces rejection in the control loop, i.e., without the DOB.
3) $Haptic^{+}\ scenario$: Same as $Haptic\ scenario$ but with the DOB and the perturbation rejection (Fig. 3).
4) $Visual \cup Haptic^{+}\ scenario$: The participant perceives the level of light intensity through a color slider and feels the variations of light intensity as in $Haptic^{+}\ scenario$.

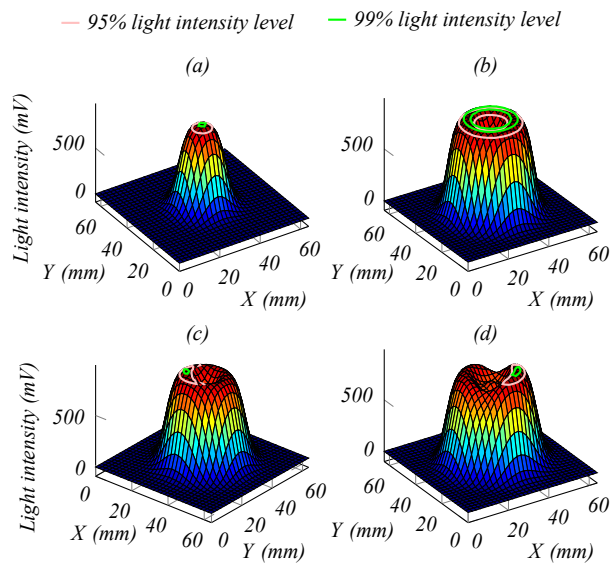

Fig. 14. Light maps used for the user evaluation.

The participant is randomly subjected to the four different light intensity distributions (Fig. 14). The participant then moves the panthograph until she/he thinks she/he has recognized the distribution, then selects the corresponding distribution. In addition, each participant is asked to locate the point (XY coordinates) that she/he believes corresponds to the maximum light intensity. The distribution identification score (0 for incorrect distribution selection, 1 for successful distribution selection) for each one, the position of the maximum light intensity selected by the participant, and the level of light intensity achieved at that position are evaluated in this study. After completing all tests, the participant ranks these four scenarios in the order she/he prefers.

D. Results

A total of 224 tests have been performed (4 tests $\times$ 4

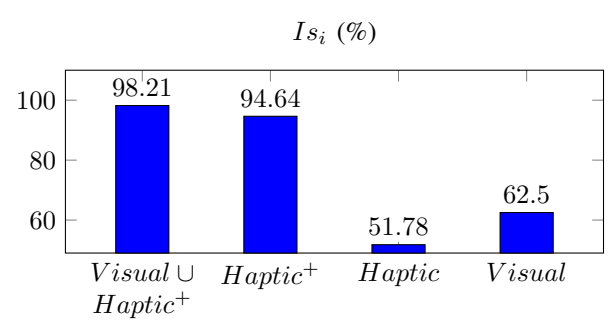

Fig. 15. Is_i in %, the success rate for light intensity maps identification for the scenario i, that represents the total of tests where the distribution is successfully identified over the total tests of the scenario i.

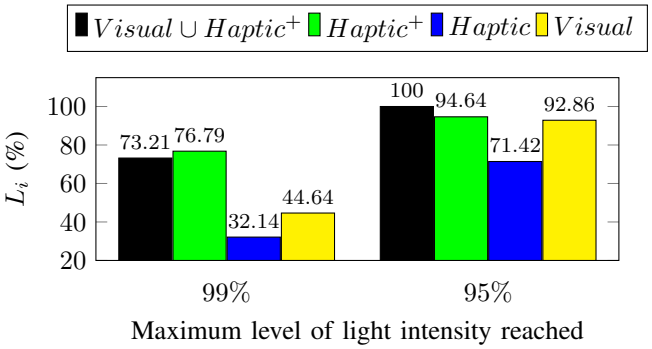

Fig. 16. L_i, the percentage of tests where the participants reach more than 95 % (nominal region of interest (region 1)) and 99 % (region 2) of the maximum light intensity with the scenario i.

scenarios $\times$ 14 participants). To evaluate the influence of the information feedback on the participant performances for such tasks, two variables are defined. Is_i in %, the success rate of distribution identification for the scenario i, that represents the total of tests where the distribution is successfully identified over the total tests for the scenario i. L_i in % represents the percentage of tests where the participant reaches more than 95 % (i.e the participant is able to successfully find a position which is in the region of interest 1) and 99 % (corresponds to the region 2 where a high quality alignment is needed) of the maximum of the light intensity over the total tests with the scenario i.

Identification of the light intensity distributions:

Fig. 15 shows the success rate of distribution identification Is_i for each scenario. With the $Visual\ scenario$, participants are able to identify correctly the light intensity distributions in 62.5% of the tests (35 tests /56). While, with $Haptic^+\ scenario$, the success rate of distribution identification of the participants is improved. The participants have successfully identified the light intensity distributions in 94.64 % of the tests. This is not the case for the $Haptic\ scenario$. Without perturbation rejection, the participant failed to distinguish the distributions where small variations are present (i.e, such as between Fig. 14 (b), (c), and (d)), which explains the decrease of the identification success rate in this scenario ($Is_{Haptic} = 51.78\%$). However, in the scenario $Visual \cup Haptic^+$, the participant successfully identifies almost all the distributions $Is_{Visual \cup Haptic^+} = 98.21\%$ (55 tests /56).

Alignment Performances:

Fig. 16 shows the percentage of tests where the participants are able to recognize the regions of interest over the total test for each scenario. Let us recall that in the region 1 and the region 2, the light intensity is more than 95 % and 99 % of its maximum value respectively.

Region 1: With the $Visual \cup Haptic^+$ scenario, all the participants succeed to position in the region of interest ($L_{Visual \cup Haptic^+}(95\%) = 100\%$). Whereas, with the visual feedback only, the participants reach the region of interest in 92.86 % of the tests. Comparing the $Visual \cup Haptic^+$ to $Visual$ scenario, the benefit of the haptic feedback with perturbation rejection on the alignment performances appears clearly. With the $Haptic^+$ scenario, the participants successfully position in the region of interest in 94.64 % of the tests. However, this percentage decreases in the $Haptic$ scenario, where the perturbation forces affect the small light intensity variation feeling ($L_{Haptic}(95\%) = 71.42\%$).

Region 2: Considering the case where a high level of light intensity transmission is required (more than 99 %), the efficiency of the haptic feedback with perturbation rejection appears significantly. With only the force feedback with perturbation rejection ($Haptic^+$ scenario), the participants successfully position in the region 2 in 76.79% of the tests. Whereas, the $Visual \cup Haptic^+$ scenario does not have a significant advantage over the $Haptic^+$ scenario ($L_{Visual \cup Haptic^+}(99\%) = 73.21\%$). Moreover, with the $Haptic$ and $Visual$, the percentage of tests where participants reach more than 99 % of the maximum light intensity doesn't exceed 32.14 % and 44.64% respectively.

TABLE I
ACCEPTABILITY STUDY FOR THE DIFFERENT SCENARIOS SHOWS THE SELECTED PREFERENCES BY THE PARTICIPANTS. IN THE FIRST COLUMN, FOR EACH ROW, SCENARIO A>SCENARIO B>SCENARIO C>SCENARIO D, MEANS THAT SCENARIO A IS PREFERRED TO SCENARIO B, THE LATER IS PREFERRED TO SCENARIO C, ANS SO ON.

Selected preferences.	# Participants
$Visual \cup Haptic^+ > Haptic^+ > Haptic > Visual$	9
$Visual \cup Haptic^+ > Visual > Haptic^+ > Haptic$	3
$Haptic^+ > Visual \cup Haptic^+ > Haptic > Visual$	1
$Visual > Haptic^+ > Haptic > Visual \cup Haptic^+$	1

E. Discussion

In general, the distribution recognition is improved by the enhanced haptic feedback with the perturbation rejection strategy ($Is_{Haptic^+} > Is_{Visual} > Is_{Haptic}$). In addition, based only on the light intensity variations feeling with the perturbation rejection, the quality of the alignment task is improved (i.e $L_{Haptic^+}(99\%) = 76.78\%$ comparing to $L_{Haptic}(99\%) = 32.14\%$ and $L_{visual}(99\%) = 44.64\%$ Fig. 16). Considering the participants' preferences summarized in TABLE I, there is a considerable agreement in the preference of the force feedback $\{Haptic^+, Haptic\}$ over the visual one $\{Visual\}$ (10/14 participants). In addition, there is a total agreement in the preference of the $\{Haptic^+\}$ over the $\{Haptic\}$ one. Whereas, only four participants prefer the $Visual$ scenario over the $Haptic^+$ scenario. Indeed, the results of these participants in the $Haptic^+$ scenario are better than those in the $Visual$ scenario. These results prove the effectiveness of the proposed approach. By relying solely on the feeling of light variations with disturbance rejection ($Haptic^+\ scenario$), the performance of the alignment task is improved over the currently used technique in the industry ($Visual\ scenario$ used in AUREA Company). Moreover, this approach has received a significant agreement from the participants, which reflects its efficiency and ease of use.

VI. CONCLUSION

In this paper, an original approach to haptic teleoperation and HRI is proposed where a light signal is used as haptic feedback. The case study concerned the alignment of a laser

on the active surface of a photodiode, with sub-micrometric accuracy, using a micro-robotic system and a pantograph. First, the effect of the pantograph transparency on the alignment accuracy of the optical fiber with haptic light feedback has been studied. It has been shown that the inertial force generated by the pantograph results in alignment errors of up to 10 μm, whereas with a DOB, this error is reduced to 0.7 μm. This is very critical because an alignment error of 1 μm can lead to a loss of more than 35 $\%$ in the light signal transmission. Second, HRI strategies have been proposed for intuitive fiber alignments. These strategies take into account the fact that a user may perform fast or slow pantograph movements for laser alignment. In both cases, a sub-μm alignment accuracy is achieved. Finally, a user evaluation is performed to quantify the interest and acceptability of the different HRI scenarios. The motivation of this work goes beyond the case study of this article. It concerns more generally the control of micro-robotic systems by haptic feedback when light information is involved in decision-making. To our knowledge, this work is the first in the literature that addresses this issue. Future works will focus on robust dynamic closed-loop control of the micro-robotic system to address position and velocity control in a wide bandwidth. The actuators used in our laboratory can be controlled at a bandwidth in the kHz range. In addition, strategies for shared human-robot control will be investigated by adding more autonomy to the robot while performing a task together with the human operator.

ACKNOWLEDGMENT

These works have been partially funded by the Bourgogne Franche-Comté région, COLAMIR project (contract "ANR-16-CE10-0009"), and the DyNaBot project (contract "ANR-21-CE10-0016"), supported by the EUR EiPHi Graduate school (contract "ANR-17-EURE-0002"), Robotex contract "ANR-10-EQPX-44-01" and the French RENATECH network through its FEMTO-ST technological facility.

REFERENCES

[1] V. Sariola, Q. Zhou, and H. N. Koivo, "Hybrid microhandling: a unified view of robotic handling and self-assembly," *Journal of Micro-Nano Mechatronics*, vol. 4, no. 1-2, p. 5, 2008.

[2] C. Clévy, I. Lungu, K. Rabenorosoa, and P. Lutz, "Positioning accuracy characterization of assembled microscale components for micro-optical benches," *Assembly Automation*, vol. 34, no. 1, pp. 69 – 77, 2014.

[3] K. Aoki, H. T. Miyazaki, H. Hirayama, K. Inoshita, T. Baba, K. Sakoda, N. Shinya, and Y. Aoyagi, "Microassembly of semiconductor three-dimensional photonic crystals," *Nature materials*, vol. 2, no. 2, pp. 117–121, 2003.

[4] K. Rabenorosoa, C. Clévy, P. Lutz, A. N. Das, R. Murthy, and D. Popa, "Precise motion control of a piezoelectric microgripper for microspectrometer assembly," in *International Design Engineering Technical Conferences and Computers and Information in Engineering Conference*, vol. 49033, pp. 769–776, 2009.

[5] M. Gauthier and S. Régnier, *Robotic Micro-assembly*. John Wiley & Sons, 2010.

[6] A. Bolopion and S. Régnier, "A review of haptic feedback teleoperation systems for micromanipulation and microassembly," *IEEE Transactions on Automation Science and Engineering*, vol. 10, no. 3, pp. 496–502, 2013.

[7] B. Komati, C. Clévy, and P. Lutz, "Force tracking impedance control with unknown environment at the microscale," in *International Conference on Robotics and Automation*, pp. 5203–5208, 2014.

[8] F. Shen, F. Qin, Z. Zhang, D. Xu, J. Zhang, and W. Wu, "Automated pose measurement method based on multivision and sensor collaboration for slice microdevice," *IEEE Transactions on Industrial Electronics*, vol. 68, no. 1, pp. 488–498, 2020.

[9] R. Oubellil, A. Voda, M. Boudaoud, and S. Régnier, "A 2-dof h∞ control strategy for a 3 axes robotic system operating at the nanometer scale," in *International Conference on System Theory, Control and Computing*, 2016.

[10] R. Oubellil, A. Voda, M. Boudaoud, and S. Régnier, "Robust control strategies of stick-slip type actuators for fast and accurate nanopositioning operations in scanning mode," in *Mediterranean Conference on Control and Automation*, 2015.

[11] M. Boudaoud, M. Gaudenzi De Faria, Y. Le Gorrec, Y. Haddab, and P. Lutz, "An output feedback lpv control strategy of a nonlinear electrostatic microgripper through a singular implicit modeling," *Control Engineering Practice*, vol. 28, pp. 97–111, 2014.

[12] M. Boudaoud, Y. Le Gorrec, Y. Haddab, and P. Lutz, "Gain scheduled control strategies for a nonlinear electrostatic microgripper: Design and real time implementation," in *IEEE Conference on Decision and Control*, 2012.

[13] J. Du, W. Sheng, and M. Liu, "A human–robot collaborative system for robust three-dimensional mapping," *IEEE/ASME Transactions on Mechatronics*, vol. 23, no. 5, pp. 2358–2368, 2018.

[14] M. Raessa, J. C. Y. Chen, W. Wan, and K. Harada, "Human-in-the-loop robotic manipulation planning for collaborative assembly," *IEEE Transactions on Automation Science and Engineering*, vol. 17, no. 4, pp. 1800–1813, 2020.

[15] C. Clévy, M. Rakotondrabe, and N. Chaillet, "Signal measurement and estimation techniques issues in the micro/nano world," 2011.

[16] D. Chen, A. Song, L. Tian, Q. Ouyang, and P. Xiong, "Development of a multidirectional controlled small-scale spherical mr actuator for haptic applications," *IEEE/ASME Transactions on Mechatronics*, vol. 24, no. 4, pp. 1597–1607, 2019.

[17] J. L. Santos and F. Farahi, *Handbook of optical sensors*. Crc Press, 2014.

[18] H. Bettahar, O. Lehmann, C. Clévy, N. Courjal, and P. Lutz, "Photo-robotic extrinsic parameters calibration of 6-dof robot for high positioning accuracy," *IEEE/ASME Transactions on Mechatronics*, vol. 25, no. 2, pp. 616–626, 2020.

[19] A. Awde, M. Boudaoud, S. Régnier, and C. Clévy, "Disturbance observer based control approach for collaborative robotics at small scales," in *International Conference on Intelligent Robots and Systems*, pp. 2872–2878, Las Vegas, USA, 2020.

[20] T. Lu, C. Pacoret, D. Hériban, A. M. Ousaid, S. Régnier, and V. Hayward, "Kilohertz bandwidth, dual-stage haptic device lets you touch brownian motion," *IEEE Transactions on haptics*, vol. 10, no. 3, pp. 382–390, 2016.

[21] A. Bolopion, B. Cagneau, S. Redon, and S. Régnier, "Comparing position and force control for interactive molecular simulators with haptic feedback," *Journal of Molecular Graphics and Modelling*, vol. 29, no. 2, pp. 280–289, 2010.

[22] A. Bolopion, B. Cagneau, D. S. Haliyo, and S. Régnier, "Analysis of stability and transparency for nanoscale force feedback in bilateral coupling," *Journal of Micro-Nano Mechatronics*, vol. 4, no. 4, pp. 145–158, 2008.

[23] A. Bolopion, B. Cagneau, S. Redon, and S. Régnier, "Variable gain haptic coupling for molecular simulation," in *IEEE World Haptics Conference*, pp. 469–474, 2011.

Ahmad Awde received the Dipl. Ing. degree in Mechanical engineering from the Lebanese Faculty of Engineering, Beyrouth, Lebanon, in 2018, and the Master's degree in Systems information technology from University of Technology of Compiègne, Compiègne, France, in 2018. He is currently working toward the PhD degree in Automatic Control and Robotics in collaboration between the Femto-St Institute, University Bourgogne-Franche-Comté and the Institute for Intelligent Systems and Robotics, Sorbonne University, France.

Mokrane Boudaoud is Associate Professor (Maitre de Conférences) at Sorbonne University, with research affiliation at ISIR - Institut des Systèmes Intelligents et de Robotique. He received the Engineering degree in Automatic Control from the University of Science and Technology Houari Boumédiène (USTHB, Algiers, Algeria), and a MS degree in Mechatronics and Microrobotics at the University of Franche-Comté (UFC, Besançon, France) in 2009. He obtained in 2012 the PhD degree in control engineering at Femto-st Institute. His main fields of interest are micro/nano-robotics, robust control and nonlinear modeling.

Mélanie Macioce graduated with a work-study master's degree from the University of Limoges, France. The subject of her studies revolves around photonics and telecommunications. She works for AUREA TECHNOLOGY as a Photonics Engineer since 2017.

Stéphane Régnier received his PhD degree in Mechanics and Robotics from the University of Pierre and Marie Curie, Paris, France in 1996. He is currently Professor at the Institute of Intelligent Systems and Robotics (ISIR), Sorbonne University, Paris, France. He has been head of the ISIR micromanipulation team since 2001. His research interests are focused on micro and nano manipulation, teleoperation and haptic feedback at the nanoscale, micromechatronics and biological cell characterization.

Cédric Clévy received his Ph.D. degree in Automatic Control and computer Sciences in 2005 from the University of Franche-Comté, France. Since 2006, he has been an Associate Professor at the University of Bourgogne Franche-Comté, Besancon, France working in the AS2M (Automatic Control and MicroMechatronic Systems) department of FEMTO-ST Institute. His research interests are the design, modeling and control of micro and nanorobotic systems for the characterisation, manipulation and assembly at micro and nanoscales. Cédric Clévy currently leads the "Micro and Nano Robotics" research team of the FEMTO-ST Institute.